Whitney edge elements and the Runge phenomenon

Ana Alonso Rodríguez, Ludovico Bruni Bruno, Francesca Rapetti

Whitney edge elements and the Runge phenomenon

Ana Alonso Rodríguez[a], Ludovico Bruni Bruno[a], Francesca Rapetti[b]

[a] *Università degli Studi di Trento, Loc. Povo, Trento (IT)*
[b] *Université Côte d'Azur, Parc Valrose, Nice (FR)*

Abstract

It is well known that Lagrange interpolation based on equispaced nodes can yield poor results. Oscillations may appear when using high degree polynomials. For functions of one variable, the most celebrated example has been provided by Carl Runge in 1901, who showed that higher degrees do not always improve interpolation accuracy. His example was then extended to multivariate calculus and in this work we show that it is meaningful, in an appropriate sense, also for Whitney edge elements, namely for differential 1-forms.

Keywords: Interpolation, differential forms, edge elements, weights, Runge phenomenon
2000 MSC: 65N30, 65D05

1. Introduction

The principal aim of this work is to generalise the Runge counterexample to the case of differential 1-forms when interpolated in the space $\mathcal{P}_r^-\Lambda^1(T)$ of high order Whitney 1-forms of polynomial degree r over an n-simplex T.

In the scalar case, Runge phenomenon may occur when two properties, one associated with the function f to be interpolated, the other with the set of evaluation points, hold simultaneously. Indeed, if the magnitude of the r-th order derivatives of f blows up as the polynomial degree r grows and the Lebesgue constant associated with the considered distribution of interpolation nodes increases quickly as well with r, the interpolation error, as a function of r, is bounded by a quantity that grows sharply. Clearly this does not necessarily imply that the error itself goes to infinity, whence the relevance of the Runge counterexample. In fact, Runge found a regular and bounded function f_R, which is a scaled version of the *Witch of Agnesi*, such that the polynomial interpolating f_R at equispaced points in a bounded interval suffers from wild oscillations near the interval extremities as its degree

r is increased. This example originated a huge amount of mathematical literature about finding possible solutions to mitigate the problem of oscillations. On the one side, distributions of nodes that minimize the Lebesgue constant were studied in any space dimension $n \geq 1$; see, for instance, [1], [2], [3], [4], [5] and the reference therein. On the other side, suitable polynomial bases were adopted in place of the canonical one, either composed of orthogonal polynomials, as in [6], [7], or by piece-wise polynomials such as splines, see [8]. Nowadays, widely used spectral and finite element methods combine in a masterful way all these aspects of polynomial interpolation, see for example [9], in order to avoid this phenomenon.

To generalise the Runge counterexample to the case of 1-forms, we first need to introduce a framework for polynomial interpolation of differential 1-forms on simplices. This approach shall reproduce and extend fundamentals concepts featuring in the classical scalar case. To this purpose *weights*, that are degrees of freedom based on integration on supports called *small simplices* [10], are invoked. Weights generalise the concept of nodal evaluations (naturally associated with 0-forms) to higher dimensional forms, and allow for the definition of an extension of the Lebesgue constant that stitches with the nodal one [11]. The last ingredient that we shall put at play is the commutativity of the diagram linking projections onto approximation spaces $\mathbb{P}_r(T)$, $\mathcal{P}_r^-\Lambda^1(T)$ and the differential operator, see [12], [13].

The structure of the paper is as follows. In Section 2 we present, as a motivation, an overview of the classical and consolidated state of the art concerning the nodal case. In Section 3 we offer the tools to extend the Runge counterexample to differential 1-forms. This section also contains the main theoretical result of the paper, which is Proposition 3.4. In Section 4 we present numerical results that are in accordance with Proposition 3.4, providing explicitly a 1-form with the desired features. Examples for $n = 1, 2, 3$ are exhibited. We gather comments and further developments in Conclusions, at the end of the paper.

2. A guiding example: the scalar case

Nodal Lagrange interpolation consists in associating a function with a polynomial of prescribed degree r that share an appropriate number of nodal evaluations. Let us denote by N the dimension of the space of polynomials of degree r and recall that in $\mathbb{R}^n$, one has $N = \binom{n+r}{n}$. For $n = 1$ one thus obtains that $N = \dim \mathbb{P}_r(\mathbb{R}) = r + 1$, and the interpolation problem can be neatly stated as follows. Consider an interval $I \doteq [a, b] \subset \mathbb{R}$ and N distinct points $z_1, \ldots, z_N$ contained in I. Suppose to know the set of evaluations $f(z_1), \ldots, f(z_N)$ of a continuous functions $f : I \to \mathbb{R}$. Then

there exists a unique polynomial p_r of degree r such that $p_r(z_j) = f(z_j)$ for $j = 1, \ldots, N$. Letting $\{\varphi_j\}_{j=1,\ldots,N}$ denote the Lagrange basis, i.e. the collection of polynomials of degree N such that $\varphi_j(z_\ell) = \delta_{j,\ell}$, the polynomial p_r may be written uniquely as

$$p_r(x) = \sum_{j=1}^{N} f(z_j)\varphi_j(x). \tag{1}$$

An estimation of the interpolation error $\|f - p_r\|_\infty \doteq \sup_{x\in I} |f(x) - p_r(x)|$ depends on the choice of points $z_1, \ldots, z_N$ via the Lebesgue constant

$$\Lambda_r \doteq \sup_{x\in I} \sum_{i=0}^{N} |\varphi_i(x)|. \tag{2}$$

In particular, one has that

$$\|f - p_r\|_\infty \leq (1 + \Lambda_r)\|f - p_r^*\|_\infty, \tag{3}$$

being p_r^* the so-called *best fit approximation*. The *Runge counterexample* [14] concerns the function $f_R : [-1, 1] \to \mathbb{R}$ defined by

$$f_R(x) \doteq \frac{1}{1 + 25x^2}. \tag{4}$$

It is well known that if equispaced points are considered as interpolation nodes, the interpolation error for f_R increase as r increase. On the contrary, other choices of nodes ensure convergence [1].

Figure 1 shows the graph of the function f_R and those of the interpolating polynomial p_r for three different values of r. On the left the interpolation nodes are equally spaced and the interpolating polynomial has near the interval extremities oscillations that increase with r. On the right the interpolation nodes are the Gauss-Lobatto ones that ensure convergence.

Examples of multivariate functions that present a similar behaviour have been studied in several papers, see [3]. When the dimension of the ambient space n is greater than 1, the usual setting becomes that of simplices, namely triangles when $n = 2$ and tetrahedra when $n = 3$. To this end, we shall consider the *standard simplex* T, *i.e.*, the n-simplex generated by the origin $\mathbf{0}$ and the n vectors $\mathbf{e}_i$, $i = 1, \ldots, n$, of the canonical basis of $\mathbb{R}^n$. Interpolator (1) is intended considering evaluations on points of the simplex and shape functions are now multivariate functions $\varphi_j(x_1, \ldots, x_n) : \mathbb{R}^n \to \mathbb{R}$. Consequently, a concept of Lebesgue constant can be provided [2]. There is not a unique natural way to extend (4) to $n > 1$. For each n, we find it convenient to consider the function $\tilde{f}_R(x_1, \ldots, x_n) : T \to \mathbb{R}$ defined in [4] by

$$\tilde{f}_R(x_1, \ldots, x_n) \doteq \prod_{i=1}^{n} \frac{1}{1 + 100\left(x_i - \frac{1}{2}\right)^2}. \tag{5}$$

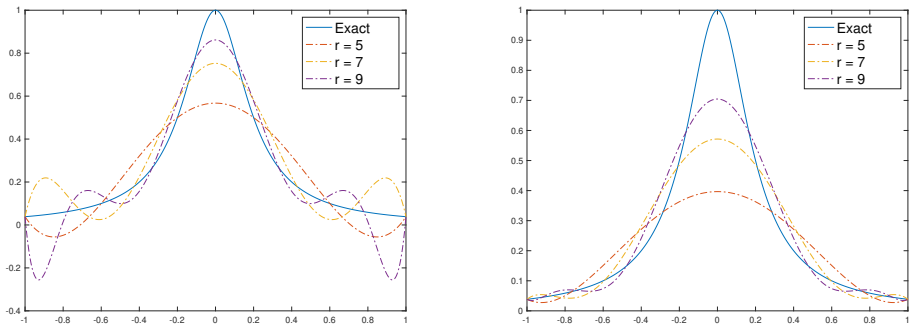

Figure 1: The Runge phenomenon for $k = 0$ on $[-1, 1]$. Continuous line represents $f(x)$ and other dashdotted lines represent $p_r(x)$ for different values of its polynomial degree r. On the left the interpolation nodes are equally spaced, on the right Gauss-Lobatto interpolation nodes are used.

3. Interpolation of differential forms

Interpolation in the space $\mathcal{P}_r^-\Lambda^k(T)$ of *trimmed polynomial differential k-forms* by means of *weights* is an interesting application of *finite element exterior calculus*. It extends the concept of Lagrangian interpolation to this framework and offers an intuitive link between the space of Whitney k-forms and measurements obtained in a concrete physical situation. Several of its feature generalise in fact usual properties of nodal Lagrangian interpolation. In this work we study Runge-like phenomena for differential 1-forms in the context of *simplicial interpolation*.

3.1. High order Whitney forms

Let T be an n-simplex generated by vertices $\{\mathbf{x}_0, \ldots, \mathbf{x}_n\}$ and denote barycentric coordinates for T by $\{\lambda_0, \ldots, \lambda_n\}$. For each increasing permutation $\sigma : \{0, \ldots, k\} \to \{0, \ldots, n\}$ we consider the k-subsimplex F_σ of T generated by $\{\mathbf{x}_{\sigma(0)}, \ldots, \mathbf{x}_{\sigma(k)}\}$ and associate the Whitney k-form

$$\omega_\sigma \doteq \sum_{i=0}^{n} (-1)^i \lambda_{\sigma(i)} \mathrm{d}\lambda_{\sigma(0)} \wedge \ldots \wedge \widehat{\mathrm{d}\lambda}_{\sigma(i)} \wedge \ldots \wedge \mathrm{d}\lambda_{\sigma(k)}, \tag{6}$$

the hat indicating that the term $\mathrm{d}\lambda_{\sigma(i)}$ is removed. Some examples of Whitney forms associated with the corresponding subsimplex of T are shown in Figure 2. Whitney forms may be expressed in terms of their proxies, *i.e.*, the dual scalar or vector fields. For $k = 0$, Whitney 0-forms are just the hat functions represented by barycentric coordinates λ_i, for $i = 0, \ldots, n$. For $k = 1$ there is a correspondence between Whitney 1-forms and vector

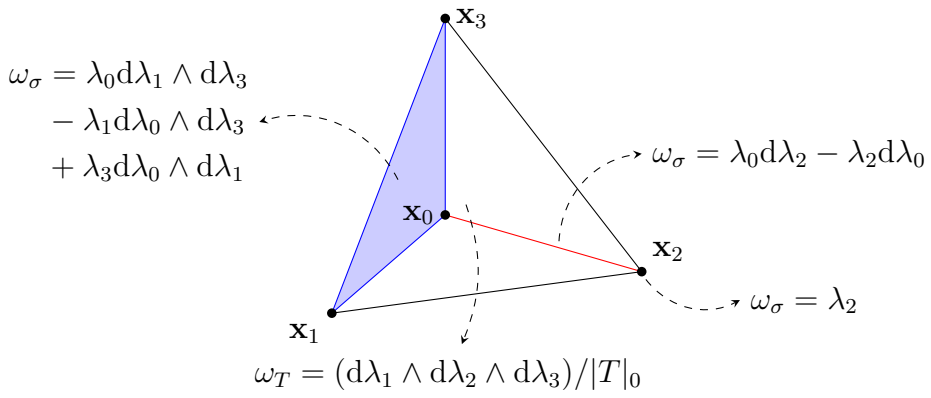

Figure 2: Examples of Whitney forms ω_σ associated with simplices σ such that $\int_\sigma \omega_\sigma = 1$.

fields that, for each edge $F_\sigma = [\boldsymbol{x}_k, \boldsymbol{x}_\ell]$ of T, associates the Whitney 1-form $\omega_\sigma = \lambda_k \mathrm{d}\lambda_\ell - \lambda_\ell \mathrm{d}\lambda_k$ with the vector field $\mathbf{w}_\sigma = \lambda_k \nabla\lambda_\ell - \lambda_\ell \nabla\lambda_k$.

Letting $\Delta_k(T)$ denote the collection of k-subsimplices of T, the space of Whitney k-forms (see [12], [13]) is

$$\mathcal{P}_1^- \Lambda^k(T) \doteq \mathrm{span}\left\{\omega_\sigma \ : \ F_\sigma \in \Delta_k(T)\right\}. \tag{7}$$

By multiplication with polynomials of degree $|\boldsymbol{\alpha}| = \alpha_0 + \ldots + \alpha_n = r - 1$ in the unknown $\boldsymbol{\lambda} = (\lambda_0, \ldots, \lambda_n)$, setting $\boldsymbol{\lambda}^{\boldsymbol{\alpha}} \doteq \lambda_0^{\alpha_0} \cdot \ldots \cdot \lambda_n^{\alpha_n}$ for each multi-index $\boldsymbol{\alpha} \in \mathcal{I}(n+1, r-1)$, we define the space of *high order Whitney forms* [10]

$$\mathcal{P}_r^- \Lambda^k(T) \doteq \mathcal{P}_{r-1}(T) \otimes \mathcal{P}_1^- \Lambda^k(T). \tag{8}$$

High order Whitney k-forms thus reads as $\boldsymbol{\lambda}^{\boldsymbol{\alpha}} \omega_\sigma$, provided that F_σ is a k-subsimplex of T. This space is equipped with the 0-norm [15], which is

$$\|\omega\|_0 \doteq \sup_{c \in \mathcal{C}^k(T)} \frac{1}{|c|_0} \left| \int_c \omega \right|, \tag{9}$$

where $\mathcal{C}^k(T)$ is the set of k-chains supported in T and $|c|_0$ is the k-th Hausdorff measure of the k-chain c. We assume that the same norm endows the space of smooth forms $\Lambda^k(T)$. The relevance of this norm in the context of Whitney forms has been pointed out in [11]. In practical applications, we shall estimate this norm by computing the maximum over a rich enough collection of k-simplices supported in T.

As degrees of freedom for the space $\mathcal{P}_r^- \Lambda^k(T)$ we consider *weights*.

Definition 3.1. *Let s be a simplex supported (i.e. topologically contained) in T. The weight associated with s and $\omega \in \mathcal{P}_r^- \Lambda^k(T)$ is*

$$\int_s \omega.$$

Weights thus assume the meaning of nodal evaluations for $k = 0$ and circulation along edges for $k = 1$. We look for collections of simplices $\{s_1, \ldots, s_N\}$, with $N = \dim \mathcal{P}_r^- \Lambda^k(T)$, that give *unisolvent* weights for the space $\mathcal{P}_r^- \Lambda^k(T)$, *i.e.* such that, for each $\omega \in \mathcal{P}_r^- \Lambda^k(T)$,

$$\int_{s_i} \omega = 0 \qquad i = 1, \ldots, N$$

implies that $\omega = 0$. A condition for unisolvence is given by the invertibility of the *generalised Vandermonde matrix*. Let $\{\omega_1, \ldots, \omega_N\}$ be a basis for $\mathcal{P}_r^- \Lambda^k(T)$ and $\{s_1, \ldots, s_N\}$ be an ordered collection of simplices. We call *generalised Vandermonde matrix* the matrix V whose (i, j)-th element is

$$V_{i,j} \doteq \int_{s_i} \omega_j. \tag{10}$$

We have the following result (see, for instance, [16]).

Lemma 3.2. *Let $\{\omega_1, \ldots, \omega_N\}$ be a basis for $\mathcal{P}_r^- \Lambda^k(T)$. The collection of k-simplices $\{s_1, \ldots, s_N\}$ is unisolvent for $\mathcal{P}_r^- \Lambda^k(T)$ if and only if the associated generalised Vandermonde matrix is invertible.*

Now, if the generalised Vandermonde matrix V is invertible, for $\mathcal{P}_r^- \Lambda^k(T)$ we may consider the basis $\{\omega_{s_1}, \ldots, \omega_{s_N}\}$ given by $\omega_{s_j} = \sum_{\ell=1}^{N} (V^{-1})_{\ell,j} \, \omega_\ell$, for $j = 1, \ldots, N$. It is immediate to check that

$$\int_{s_i} \omega_{s_j} = \delta_{i,j},$$

and we call $\{\omega_{s_1}, \ldots, \omega_{s_N}\}$ the *cardinal basis* for $\mathcal{P}_r^- \Lambda^k(T)$. It plays the role of shape function set. Hence, if $\{s_1, \ldots, s_N\}$ induces a family of unisolvent weights for $\mathcal{P}_r^- \Lambda^k(T)$, we may define an interpolator by means of weights as

$$\begin{aligned} \Pi_r^k : \quad & \Lambda^k(T) \to \mathcal{P}_r^- \Lambda^k(T) \\ & \omega \mapsto \sum_{i=1}^{N} \left(\int_{s_i} \omega \right) \omega_{s_i}. \end{aligned} \tag{11}$$

This definition is well posed [17]. We have the following property, that holds for moments as well, as shown in [13].

Proposition 3.3. *Consider a unisolvent set $\{s_1, \ldots, s_N\}$ of 1-simplices such that $s_i = [\boldsymbol{x}_{i(0)}, \boldsymbol{x}_{i(1)}]$ and the associated interpolation operators Π_r^1 and Π_r^0. Then the diagram*

$$\begin{array}{ccc} \Lambda^0(T) & \xrightarrow{\mathrm{d}} & \Lambda^1(T) \\ \downarrow{\scriptstyle \Pi_r^0} & & \downarrow{\scriptstyle \Pi_r^1} \\ \mathcal{P}_r^-\Lambda^0(T) & \xrightarrow{\mathrm{d}} & \mathcal{P}_r^-\Lambda^1(T) \end{array}$$

commutes.

Proof. We want to show that $\mathrm{d}\left(\Pi_r^0\omega\right) = \Pi_r^1(\mathrm{d}\omega)$ for each $\omega \in \Lambda^0(T)$. First, as proved in [13], one has $\mathrm{d}\left(\Pi_r^0\omega\right) \in \mathcal{P}_r^-\Lambda^1(T)$, hence $\mathrm{d}\left(\Pi_r^0\omega\right) = \Pi_r^1\left(\mathrm{d}\left(\Pi_r^0\omega\right)\right)$. Using definition (11) of interpolator and Stokes theorem, for each $\omega \in \Lambda^0(T)$, one has

$$\begin{aligned} \mathrm{d}\left(\Pi_r^0\omega\right) = \Pi_r^1\left(\mathrm{d}\left(\Pi_r^0\omega\right)\right) &= \sum_{i=1}^{N}\left(\int_{s_i}\mathrm{d}\left(\Pi_r^0\omega\right)\right)\omega_{s_i} \\ &= \sum_{i=1}^{N}\left(\Pi_r^0\omega(\boldsymbol{x}_{i(1)}) - \Pi_r^0\omega(\boldsymbol{x}_{i(0)})\right)\omega_{s_i} \qquad \text{(Stokes theorem)} \\ &= \sum_{i=1}^{N}\left(\omega(\boldsymbol{x}_{i(1)}) - \omega(\boldsymbol{x}_{i(0)})\right)\omega_{s_i} \qquad (\Pi_r^0\omega \text{ interpolates } \omega) \\ &= \sum_{i=1}^{N}\left(\int_{s_i}\mathrm{d}\omega\right)\omega_{s_i} = \Pi_r^1(\mathrm{d}\omega), \end{aligned}$$

that concludes the proof. □

Exploiting this commutativity, we may show the following result.

Proposition 3.4. *Let $\{s_1, \ldots, s_N\}$ be a unisolvent set for $\mathcal{P}_r^-\Lambda^k(T)$ and Π_r^1 be the associated interpolation operator. There exists $\alpha > 0$ such that*

$$\|\mathrm{d}\omega - \Pi_r^1\mathrm{d}\omega\|_0 \geq \alpha\|\omega - \Pi_r^0\omega\|_0. \tag{12}$$

Proof. We begin by expanding the left hand side of (12) exploiting the commutativity of the diagram proved in Proposition 3.3 and Stokes theorem:

$$\begin{aligned} \|\mathrm{d}\omega - \Pi_r^1\mathrm{d}\omega\|_0 &= \|\mathrm{d}\omega - \mathrm{d}\Pi_r^0\omega\|_0 \\ &= \sup_{c\in\mathcal{C}^1(T)}\frac{1}{|c|_0}\left|\int_c \mathrm{d}\omega - \mathrm{d}\Pi_r^0\omega\right| \\ &= \sup_{c\in\mathcal{C}^1(T)}\frac{1}{|c|_0}\left|\int_c \mathrm{d}\left(\omega - \Pi_r^0\omega\right)\right| \\ &= \sup_{c\in\mathcal{C}^1(T)}\frac{1}{|c|_0}\left|\int_{\partial c}\omega - \Pi_r^0\omega\right|. \end{aligned} \tag{13}$$

Given a 1-simplex e supported in T, let us denote by ∂e_i and ∂e_f the endpoints of the edge e. Recall that $X^0_{r,min}(T)$ is the set of interpolation nodes. We define the non empty subset of $\mathcal{C}^1(T)$ given by

$$\mathcal{C}^1_0(T) \doteq \left\{ e \in \mathcal{C}^1(T) \ : \ e \text{ is a 1-simplex and } \partial e_i \in X^0_{r,min}(T) \right\}. \tag{14}$$

Now, let us denote by L the length of the longest 1-simplex supported in T, which coincides with the length of the longest edge of the simplex T. Since $\mathcal{C}^1_0(T) \subset \mathcal{C}^1(T)$ and $L \geq |e|_0$ for each $e \in \mathcal{C}^1_0(T)$, we may bound (13) as

$$\begin{aligned}
&\sup_{c\in\mathcal{C}^1(T)} \frac{1}{|c|_0} \left| \int_{\partial c} \omega - \Pi^0_r\omega \right| \geq \sup_{e\in\mathcal{C}^1_0(T)} \frac{1}{|e|_0} \left| \int_{\partial e} \omega - \Pi^0_r\omega \right| \\
&\geq \frac{1}{L} \sup_{e\in\mathcal{C}^1_0(T)} \left| \int_{\partial e} \omega - \Pi^0_r\omega \right| \\
&= \frac{1}{L} \sup_{e\in\mathcal{C}^1_0(T)} \left| \left(\omega - \Pi^0_r\omega\right)(\partial e_f) - \left(\omega - \Pi^0_r\omega\right)(\partial e_i) \right| \\
&= \frac{1}{L} \sup_{e\in\mathcal{C}^1_0(T)} \left| \left(\omega - \Pi^0_r\omega\right)(\partial e_f) \right| \qquad \text{(because } \partial e_i \in X^0_{r,min}(T)\text{)} \\
&= \frac{1}{L} \sup_{\boldsymbol{x}\in T} \left| \left(\omega - \Pi^0_r\omega\right)(\boldsymbol{x}) \right| \qquad \text{(because } \partial e_f \text{ can be any } \boldsymbol{x} \in T\text{)} \\
&= \frac{1}{L} \|\omega - \Pi^0_r\omega\|_0.
\end{aligned}$$

The claim is thus proved for $\alpha = \frac{1}{L}$. □

4. A Runge-like counterexample for 1-forms

As a consequence of Proposition 3.4, we expect to have a Runge-like behaviour for the 1-form $\mathrm{d}f$ if the function $f(x_1, \ldots, x_n)$ offers it, provided that the weights of $\mathrm{d}f$ are computed on small edges with endpoints in nodes where f has been interpolated. A detailed construction of these families can be found in [16]. We thus consider the function $\tilde{f}_R$ defined in (5), whose differential is denoted by ω_R and reads

$$\omega_R = \mathrm{d}\tilde{f}_R = -\sum_{i=1}^{n} \left(\prod_{\substack{j=1 \\ j\neq i}}^{n} \frac{1}{1 + 100\left(x_j - \frac{1}{2}\right)^2} \right) \frac{200\left(x_i - \frac{1}{2}\right)}{\left(1 + 100\left(x_i - \frac{1}{2}\right)^2\right)^2} \mathrm{d}x_i. \tag{15}$$

For $n = 2$ and $n = 3$, we interpolate ω_R by means of the interpolator (11) and measure the quantity $\|\omega_R - \Pi^1_r\omega_R\|_0$. In both cases we consider 1-simplices

whose endpoints are nodes that are well known and widely studied in nodal interpolation: uniform distribution of nodes, for which we expect to have a discouraging behaviour, and some non uniform ones, in particular symmetrised Lobatto [18] and warp and blend [19]. Our choice is driven by several reasons: among others, they allow for comparisons with well established results in literature for the case $k = 0$, and they are also provided with an explicit implementation strategy. For a formal definition of such nodes we address the reader to [19] and for the corresponding construction of edges we refer to [17].

Case $n = 1$

When $k = n$, k-forms are identified with functions as well. This allows to plot their graph and yields more evident and straightforward comparisons. For this reason we begin with $k = 1$ in the one dimensional space $\mathbb{R}$. In Section 2 we recalled the classical Runge phenomenon for functions of one variable, considering equidistributed nodes and comparing them with Gauss-Lobatto nodes on $[-1, 1]$. To obtain the corresponding edges, we increasingly order interpolation points $-1 = z_1 < \ldots < z_N = 1$ and define the i-th 1-simplex of $S^1_r([-1, 1])$ as $s_i \doteq [z_i, z_{i+1}]$. For $k = 0$, we considered the function in (4) and depicted the corresponding results in Figure 1.

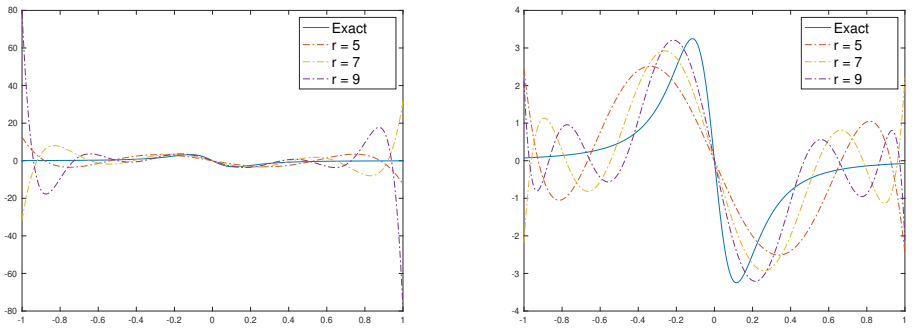

Figure 3: The Runge phenomenon for $k = 1$ on $[-1, 1]$. Continuous line represents $\omega_R(x) = \mathrm{d}f_R(x)$ and other dashdotted lines represent $\Pi^1_r\omega_R(x)$ for different values of its polynomial degree r. On the left the interpolation edges are uniform, on the interpolation edges join Gauss-Lobatto interpolation nodes. Notice the different scales in the two plots.

To study the generalisation to 1-forms we thus consider $\omega_R = \mathrm{d}f_R$, with f_R defined in (4) for $n = 1$, which reads

$$\omega_R = -\frac{50x}{\left(1 + 25x^2\right)^2}\mathrm{d}x.$$

Figure 3 shows the graph of the function ω_R and the graphs of $\Pi^1_r\omega_R$ for different values of r. Similarly to Figure 1, on the left the interpolation edges

are associated to equally spaced nodes and on the right they are associated to Gauss-Lobatto nodes. The behaviour shown if Figure 3 is consistent with that of Figure 1. When using equally spaced nodes to generate the interpolation edges, $\Pi_r^1\omega_R$ shows spurious oscilations near the interval extremities that increase as r grows. These oscillations are mitigated if one considers interpolation edges associated to the Gauss-Lobatto nodes. In particular, as r grows, the interpolated based uniform nodes diverges, whereas that associated with Gauss-Lobatto nodes converges (notice the different scales in the two plots).

Case $n = 2$

Now we consider the interpolation of 1-forms in two dimensions. This is the first case that involves vector fields.

Table 1: Estimated values of $||\omega_R - \Pi_r^1\omega_R||_0$ for different choices of interpolation edges in the standard triangle $T \subset \mathbb{R}^2$. One has $||\omega_R||_0 \approx 6.1780$.

	uniform	nonuniform	
r	$X^1_{r,min}(T)$	Sym. Lob.	W. & B.
1	6.1780	6.1780	6.1780
2	5.8321	5.8321	5.8321
3	6.1589	6.3688	6.3688
4	10.4998	7.9410	7.9412
5	5.5007	7.4914	7.5036
6	30.0759	9.0244	9.1716
7	7.6069	10.0007	10.5262
8	83.4601	8.7156	9.1573
9	25.8527	9.8961	10.7132
10	221.5058	7.3763	7.8910
11	76.7774	8.1094	8.6649
12	564.4799	5.4443	5.6343

We thus study the edge case in the standard 2-simplex $T = [\mathbf{0}, \mathbf{e}_1, \mathbf{e}_2]$. For a formal construction of small edges we refer to [16] and for a depiction of the nodal case we address the reader to [3]. We consider a mesh $\mathcal{T}_2$ generated by the software `Triangle` that presents 513 edges with length between 0.011 and 0.120. We estimate the 0-norm of any 1-form ω as

$$||\omega||_0 \approx \max_{e \in E(\mathcal{T}_2)} \frac{1}{|e|_0} \left| \int_e \omega \right|, \tag{16}$$

being $E(\mathcal{T}_2)$ the set of edges in $\mathcal{T}_2$. In particular, for $\omega_R = \mathrm{d}\tilde{f}_R$ as in (15), one obtains $||\omega_R||_0 \approx 6.1780$. The estimated values of $||\omega_R - \Pi_r^1\omega_R||_0$ for different values of r are presented in Table 1 and depicted in Figure 4. In

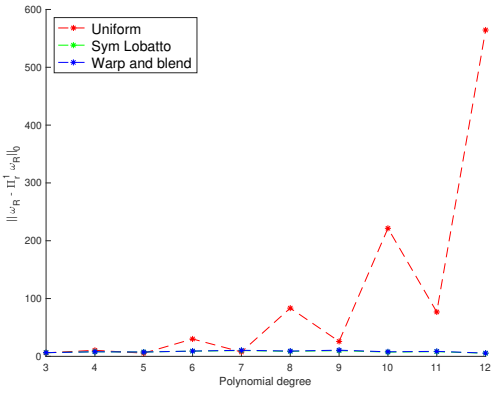

Figure 4: A graphical representation of Table 1 with respect to the polynomial degree r.

particular we consider three different distributions of interpolation edges, all of them constructed from well known distributions of interpolation nodes: the uniform distribution, the symmetrised Lobatto points and the warp and blend ones. As expected and predicted by Proposition 3.4, interpolation based on uniform small simplices offers very discouraging results. The choice of non uniform distribution of small simplices, based on symmetrised Lobatto or warp and blend nodes, mitigates this fact.

Case $n = 3$

The last example concerns 1-forms in three dimensions.

Table 2: Estimated values of $||\omega_R - \Pi^1_r \omega_R||_0$ for different choices of interpolation edges in the standard tetrahedron $T \subset \mathbb{R}^3$. One has $||\omega_R||_0 \approx 0.2957$.

	uniform	nonuniform	
r	$X^1_{r,min}(T)$	Sym. Lob.	W. & B.
1	0.2957	0.2957	0.2957
2	0.2530	0.2530	0.2530
3	0.2811	0.2881	0.2881
4	0.3217	0.3154	0.3154
5	0.2595	0.3074	0.3139
6	0.7225	0.3628	0.3798
7	0.4413	0.4282	0.4363
8	1.5092	0.3563	0.3763
9	0.9098	0.4279	0.4514
10	2.8976	0.3086	0.3231
11	1.9482	0.3744	0.3792
12	5.1180	0.2461	0.2480

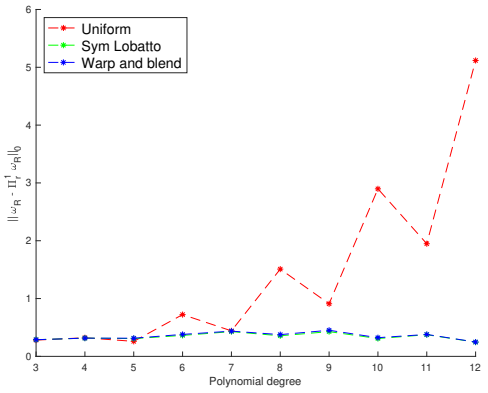

Figure 5: A graphical representation of Table 2 with respect to the polynomial degree r.

In the three dimensional context we obtain results that are comparable with those just shown for the standard triangle. In this case we consider the standard tetrahedron $T = [\mathbf{0}, \mathbf{e}_1, \mathbf{e}_2, \mathbf{e}_3]$. Again, for the selection of the edges associated with the interpolation nodes we refer to [16]. We consider a test mesh $\mathcal{T}_3$ with 13800 edges supported in T. Their length varies between 0.0435 and 0.0615. Considering ω_R as in (15) and estimating $||\omega_R||_0$ as in (16) with $\mathcal{T}_3$ in place of $\mathcal{T}_2$, we have that $||\omega_R||_0 \approx 0.2957$. The estimated values of $||\omega_R - \Pi_r^1 \omega_R||_0$ for different values of r are presented in Table 2 and depicted in Figure 5. As in the case $n = 2$ we consider distributions of interpolation edges associated with the uniform, symmetrised Lobatto and warp and blend distributions of nodes. Results are in accordance with the theory of Section 3. Once more we see that results associated with edges built on points adopted in nodal interpolation for reducing the Lebesgue constant strongly contain the Runge phenomenon, but they seem far from being optimal. Note that the field defined in (15) for $n = 2$ reaches the maximum of its magnitude on the boundary of the standard 2-simplex, while for $n = 3$ such a maximum is reached outside the standard 3-simplex. This justifies the fact that values in Table 2 are smaller than those in Table 1.

Conclusions

Tables 1 and 2 and the corresponding depictions (Figures 4 and 5, respectively) show that uniform small simplices do not offer good interpolation properties. This is in accordance with the nodal case and verifies results presented in [17] concerning the generalised Lebsgue constant. However, even non-uniform distributions of nodes, which work correctly for the interpolation of scalar fields, are not so efficient when used as extremities of the

small edges where the interpolation of 1-forms is located. From the analysis presented in these pages, it seems that we are able to generalise the Runge phenomenon from the interpolation of scalar fields to that of 1-forms, but, contrary to the nodal case, not a possible solution to mitigate it with edge unknowns. A search for optimal small simplices is a work in progress.

References

[1] P. L. Tchebychef, Oeuvres. Tomes I, II, Chelsea Publishing Co., New York, 1962.

[2] T. Bloom, The Lebesgue constant for Lagrange interpolation in the simplex, J. Approx. Theory 54 (3) (1988) 338–353.

[3] M. J. Roth, Nodal configurations and voronoi tessellations for triangular spectral elements, Ph.D. thesis, University of Victoria (2005).

[4] M. G. Blyth, H. Luo, C. Pozrikidis, A comparison of interpolation grids over the triangle or the tetrahedron, J. Eng, Math. 56 (2006) 263–272.

[5] J. S. Hesthaven, From electrostatics to almost optimal nodal sets for polynomial interpolation in a simplex, SIAM J. Numer. Anal. 35 (2) (1998) 655–676.

[6] J. S. Hesthaven, C. H. Teng, Stable spectral methods on tetrahedral elements, SIAM J. Sci. Comp. 21 (6) (2000) 2351–2380.

[7] R. Pasquetti, F. Rapetti, Spectral element methods on unstructured meshes: which interpolation points?, Numer. Algorithms 55 (2-3) (2010) 349–366.

[8] K. E. Atkinson, An introduction to numerical analysis, 2nd Edition, John Wiley & Sons, Inc., New York, 1989.

[9] C. Canuto, M. Hussaini, A. Quarteroni, T. Zang, Spectral Methods, Scientific Computation, Springer, Berlin, Heidelberg, 2006.

[10] F. Rapetti, A. Bossavit, Whitney forms of higher degree, SIAM J. Numer. Anal. 47 (3) (2009) 2369–2386.

[11] A. Alonso Rodríguez, F. Rapetti, On a generalization of the Lebesgue's constant, J. Comput. Phys. 428 (2021) 109964.

[12] A. Bossavit, Computational electromagnetism, Electromagnetism, Academic Press, Inc., San Diego, CA, 1998, variational formulations, complementarity, edge elements.

[13] D. N. Arnold, R. S. Falk, R. Winther, Finite element exterior calculus, homological techniques, and applications, Acta Numer. 15 (2006) 1–155.

[14] C. Runge, Über empirische Funktionen und die Interpolation zwischen äquidistanten Ordinaten, Zeitschrift fur Mathematik und Physik 46 (1901) 224–243.

[15] J. Harrison, Continuity of the integral as a function of the domain, Journal of Geometric Analysis 8 (5) (1998) 769–795.

[16] L. Bruni Bruno, Weights as degrees of freedoom for high order whitney finite elements, Ph.D. thesis, University of Trento (2022).

[17] A. Alonso Rodríguez, L. Bruni Bruno, F. Rapetti, Towards nonuniform distributions of unisolvent weights for Whitney finite element spaces on simplices: the edge element case, Calcolo 59 (37) (2022).

[18] M. G. Blyth, C. Pozrikidis, A Lobatto interpolation grid over the triangle, IMA J. Appl. Math. 71 (2005) 153–169.

[19] J. S. Hesthaven, T. Warburton, Nodal discontinuous Galerkin methods, Vol. 54 of Texts in Applied Mathematics, Springer, New York, 2008.